Diboride compounds doped with transition metals: A route to superconductivity through structure stabilization as well as defects

P. M. Dee,[1,2,*] J. S. Kim,[1,*] A. C. Hire,[2,3] J. Lim,[1] L. Fanfarillo,[1,4] S. Sinha,[1] J. J. Hamlin,[1] R. G. Hennig,[2,3] P. J. Hirschfeld,[1] and G. R. Stewart[1]

[1]*Department of Physics, University of Florida, Gainesville, Florida 32611, USA*

[2]*Department of Materials Science and Engineering, University of Florida, Gainesville, Florida 32611, USA*

[3]*Quantum Theory Project, University of Florida, Gainesville, Florida 32611, USA*

[4]*Scuola Internazionale Superiore di Studi Avanzati, Via Bonomea 265, 34136 Trieste, Italy*

(Received 16 October 2023; accepted 21 February 2024; published 22 March 2024)

Recent investigations into MoB_2 have unveiled a direct connection between a pressure-induced structural transition to a $P6/mmm$ space group structure and the emergence of superconductivity, producing critical temperatures up to 32 K at 100 GPa. This pressure-induced superconducting state underscores the potential of doped MoB_2 as a possible candidate for metastable superconductivity at ambient pressure. In this work, we demonstrate that doping by Zr, Hf, or Ta stabilizes the $P6/mmm$ structure at ambient pressure and results in the realization of a superconducting state with critical temperatures ranging from 2.4 up to 8.5 K depending on the specific doping. We estimate the electron-phonon coupling λ and the density of states based on resistivity and specific heat data, finding that λ ranges from 0.4 to 0.6 for these compounds. Finally, to investigate the role of possible metastable defect structures on the critical temperature, we analyze MoB_2, $MoB_{2.5}$, and Nb/Zr-doped MoB_2 using rapid cooling techniques. Notably, splat quenching produces samples with higher critical temperatures and even retains superconductivity in MoB_2 at ambient pressure, achieving a critical temperature of 4.5 K.

DOI: 10.1103/PhysRevB.109.104520

I. INTRODUCTION

The 2001 discovery of high-temperature superconductivity in MgB_2 [1] reignited what had, until that point, been a latent interest in the superconducting properties of diborides. The resulting wave of new investigations explored alternatives to Mg using transition metals (TMs). Despite a broad sampling of TMs, the pursuit failed to unearth a worthy competitor. Similar to the findings of much earlier work [2–4], many of these TM diborides were not superconductors or had critical temperatures T_c below 10 K. As it stands, MgB_2 still retains the highest measured T_c of any diboride at 39 K. However, a recent study of MoB_2 has come surprisingly close to this title, with $T_c = 32$ K at high pressure [5].

At ambient pressure, MoB_2 has no apparent superconductivity down to 1.8 K, and unlike MgB_2, every other boron layer is buckled ("puckered"), leading to the $R\bar{3}m$ [166] space group structure instead of the $P6/mmm$ [191] phase observed in MgB_2. However, above 20 GPa of applied pressure, a finite T_c emerges, ascending sharply at a rate of 0.7 K/GPa with increasing pressure until the system undergoes a structural phase transition to the P6/mmm phase near 70 GPa. Thereafter, the dT_c/dP rate drops to 0.1 K/GPa, with T_c eventually reaching 32 K near 100 GPa [5]. This hitherto unseen behavior in TM diborides raises questions about superconductivity in MoB_2 and whether it can be manipulated by pressure-induced metastability or partial substitutions with other TMs.

Early work by Cooper *et al.* [3] investigated the possibility of superconductivity in MoB_2 and several intermetallic boride compounds containing elements in the series Y, Zr, Nb, and Mo, mostly with boron concentrations above 2 compared with stoichiometric diborides. This exploration was partially motivated by the notion of an optimal electron/atom (e/at.) ratio for superconductivity in these compounds. They claimed to find a correlation between the maximum observed T_c's and an e/at. of 5–7. However, they did not observe superconductivity in either stoichiometric NbB_2 or MoB_2, even when the latter was synthesized using splat-quenching techniques. Only in the presence of excess boron—nominally reported as $NbB_{2.5}$ and $MoB_{2.5}$—did they find superconductivity, measuring the onset of T_c to be 6.4 and 8.1 K, respectively. They further explored various alloyed diboride compounds by partially substituting Mo with another metal M with nominal compositions given by $Mo_{2-x}M_xB_5$, finding T_c's ranging from 4.5 to 11.2 K (the latter corresponding to $Mo_{1.69}Zr_{0.31}B_5$).

The role of TM substitution in stabilizing the AlB_2-type structure in MoB_{2+y} was further established by Muzzy *et al.* [6]. Using Zr substitution near 4%, they created MoB_2 alloys in a metastable AlB_2 structure, obtaining compositions of the form $(Zr_{0.04}Mo_{0.96})_xB_2$. By increasing the ratio of excess boron, they found that the samples harbored more metal vacancies, and the stoichiometric diboride phase showed evidence of c-axis stacking defects. Detecting the superconducting T_c from magnetometer measurements of the magnetization in an applied field, they found that T_c increases from about 5.9 K for $x = 1.0$ to 8.2 K for $x = 0.85$. In addition to having the lowest T_c, the stoichiometric compound

*These authors contributed equally to this work.

$Zr_{0.04}Mo_{0.96}B_2$ had the broadest transition, which the authors attributed to stacking defects and associated strains.

Recent studies have explored the effects of Sc [7] and Nb [8,9] substitutions in compounds of the form $(M_yMo_{1-y})_xB_2$. Like Zr, Sc and Nb possess fewer d electrons than Mo, which results in a weaker overlap between the d_{z^2} orbitals across TM layers and between the TM layer and adjacent boron sublattice. Consequently, the bond strength between boron atoms diminishes, expanding the intralayer boron atom separation and causing the alternating puckered boron layers present in the rhombohedral phase of MoB_2 to flatten [10]. In the study by Yang *et al.* [7], the metal-deficient composition $(Sc_{0.05}Mo_{0.95})_{0.71}B_2$ displayed a critical field H_{c2} of 6.7 T, approaching the value of 9.4 T observed in MoB_2 at 110 GPa [5]. However, its maximum T_c was only 7.9 K, considerably lower than the high-pressure measurement of 32 K in MoB_2. In the Nb-substituted system, Nb doping of 25% yielded the highest ambient pressure T_c (onset) and H_{c2} at 8.15 K and 6.7 T, respectively [8]. Our subsequent high-pressure study [9] on this system showed that T_c *decreases* from 8 to 4 K between 0 and 50 GPa, followed by a steady, yet subtle, climb to 5 K at 171 GPa.

In this paper, we report and compare results on the superconductivity in MoB_2-based systems using several approaches. The first approach further explores TM substitution in arc-melted compositions of the form $(Mo_{1-y}M_y)_xB_2$, where M is Zr, Hf, and Ta (Sec. III). All of these alloys are stable in the $P6/mmm$ [191] phase with $(Mo_{0.96}Zr_{0.04})_{0.85}B_2$ yielding the highest T_c at 8.60 K. The second approach is to decrease the cooling time during sample preparation. In this direction, we synthesized the TM-doped compositions mentioned above, as well as $Nb_{0.25}Mo_{0.75}B_2$, MoB_2, and $MoB_{2.5}$, using rapid cooling/quenching techniques (Sec. IV). Details of our water-cooled splat-quenching procedure and apparatus can be found in Sec. II. Surprisingly, the rapidly cooled/quenched MoB_2 samples superconduct at ambient pressure with T_c's near 4.5 K. This is an observation of superconductivity in MoB_2 at ambient pressure, possibly enabled by the creation of $P6/mmm$-like defects during the rapid cooling process.

II. METHODS

A. Sample preparation and characterization

For experimental measurements, $(Ta/Zr/Hf)_{1-x}Mo_xB_2$ ($x = 0.04, 0.10, 0.25, 0.4, 0.5$) samples were formed by arc melting together the constituent elements. Mo foil (thickness of 0.1 mm, 99.97% from AESAR) was used to wrap the other elements. Otherwise, boron (an insulator) sometimes breaks into small pieces when heated by the plasma arc. A reasonable estimate for the temperature range for arc melting the constituent elements is between 2400 and 2700 °C. Despite the high melting point of Mo (2622 °C), the low vapor pressures of both B and Ta/Zr/Hf at this temperature led to negligible mass loss upon melting the constituents together, remelting twice.

Resistivity samples were cut from an arc-melted button using a low-speed diamond saw to dimensions of approximately $0.5 \times 0.5 \times 0.6$ mm^3. The sample was roughly rectangular with uniform thickness for the measurements. Small-scale errors arising from these assumptions were not taken into consideration. A current of no more than 0.1 mA was applied for all resistive measurements on the samples. In a separate set of measurements, resistivity bars (ρ bars) were made using a water-cooled caster to create a uniform thin bar with uniform dimensions of approximately $1 \times 1 \times 4$ mm^3. These ρ bars were cooled faster ($\sim 10^4$ °C/s) than the arc-melted button (~ 10 °C/s), which could take minutes to cool down from the melting point (e.g., 2000 °C). Resistivity measurements were done using the standard four-point probe method using a Keithley 220 programmable current source and a Keithley 2001 multimeter. Specific heat at low temperatures was measured using a standard time constant methodology [11].

X-ray diffraction (XRD) measurements were conducted using a Panalytical XPert Powder system to identify the phases present in our crystalline sample. The material was initially fragmented into small pieces before being finely ground to ensure homogeneity. After measurement, the observed XRD pattern was cross-referenced with calculated patterns from the Materials Project database [12] for accurate phase identification.

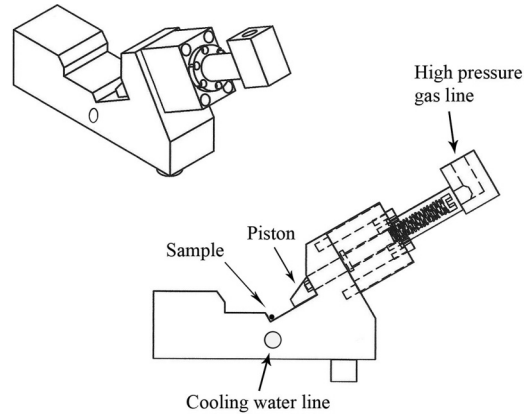

FIG. 1. Schematic design of the splat-quench device. A high-pressure gas line is fed to a solenoid valve controlling a piston. The sample is seated at the base of the copper block, just above a channel fed by a water line for rapid cooling.

B. Splat quenching

We designed and constructed a splat-quenching device (see Fig. 1) to rapidly cool thin foil samples. This device consists of a copper block with a cooling water tube running through the block below the sample. It is securely affixed to the copper hearth of our arc melter, ensuring stability during the quenching process. The design facilitates the close positioning of the arc-melter tip to the sample without interfering with other device components.

The thin foil samples were produced by momentarily pressing a molten specimen using a piston arm powered by high-pressure argon gas (200 psi) through a solenoid valve. We utilized small samples (with a diameter of less than 1 mm in their molten state) to ensure efficient melting and rapid cooling.

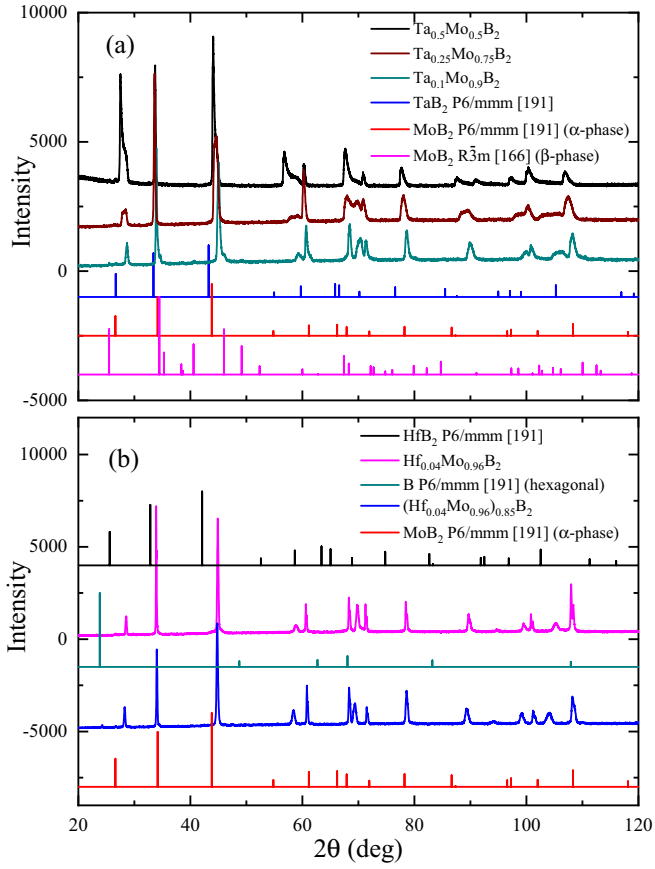

FIG. 2. X-ray diffraction measurements for (a) Ta- and (b) Hf-substituted MoB_2 prepared by an arc-melting synthesis procedure. We have included several relevant theoretical XRD results for easier comparison.

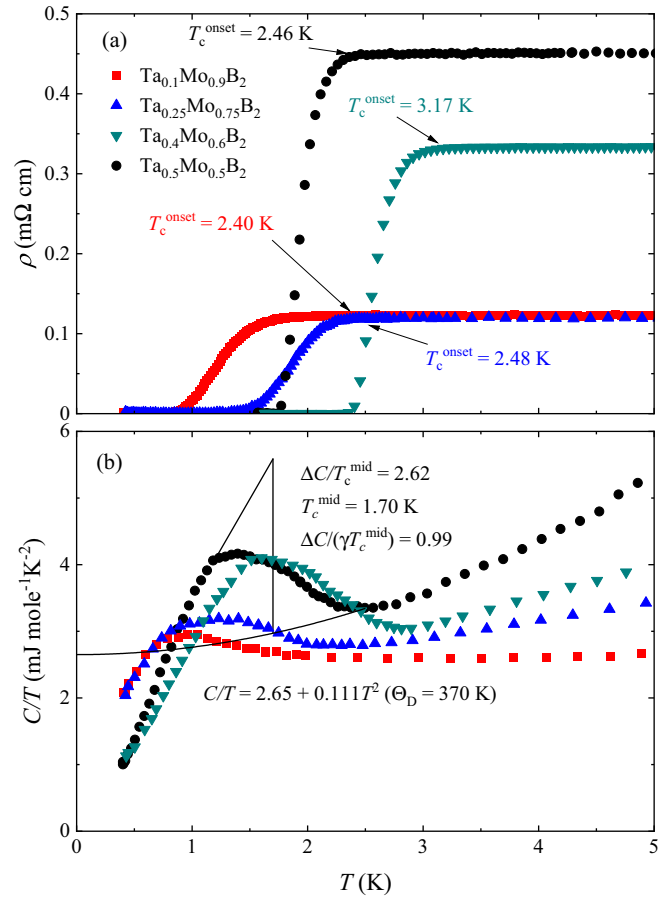

FIG. 3. Experimental results for the $Ta_{1-x}Mo_xB_2$ system for $x = 0.1$, 0.25, 0.4, and 0.5. (a) shows the resistivity measurements (in mΩ cm), and (b) shows the specific heat per unit temperature (in mJ mol^{-1} K^{-2}) for each composition. In (b), a black line is included to show an example of the Debye model fit obtained for the $x = 0.5$ composition.

III. RESULTS FOR ARC-MELTED SAMPLES

A. X-ray diffraction

Figure 2 shows the XRD results for the Ta- and Hf-doped MoB_2 compounds. Several relevant theoretical XRD patterns are shown for better comparison. These samples are best characterized as having the *P6/mmm* [191] space group structure and are closer in alignment to the MoB_2 *P6/mmm* [191] phase than that of TaB_2 or HfB_2. As expected, with higher Ta substitution approaching 50%, the XRD pattern shifts toward TaB_2. Additional XRD results for Ta- and Zr-substituted MoB_2 are shown in the Supplemental Material in Figs. S1 and S2, respectively.

B. Resistivity measurements

Resistivity and specific heat measurements were performed on all samples. The main results for $Ta_xMo_{1-x}B_2$, with $x = 0.1$, 0.25, 0.4, 0.5, are featured in Fig. 3, while the remaining results for $(Zr_{0.04}Mo_{0.96})_yB_2$ and $(Hf_{0.04}Mo_{0.96})_yB_2$ for $y = 0.85$, 1.0 are shown in Fig. 4. Resistivity measurements for each of the Ta-doped samples are shown in Fig. 3(a) up to 5 K. Additional resistivity data up to 300 K are shown in Fig. S4 of the Supplemental Material. The onset temperature of each superconducting transition T_c^{onset} was determined from the initial drop of the resistivity and found to be 2.40, 2.48, 3.17, and 2.46 K for nominal dopings $x = 0.1$, 0.25, 0.4, and 0.5, respectively. The sharpest transition relative to T_c^{onset} is seen in $Ta_{0.5}Mo_{0.5}B_2$, in contrast, with 10% and 25% Ta-doped samples. These trends are in accordance with the specific heat jumps, as shown in Fig. 3(b). The residual resistivity ratios (RRRs) $[R(300\,K)/R(T_c^{onset})]$ for $x = 0.1$, 0.25, 0.4, and 0.5 are 1.29, 1.13, 1.09, and 1.09, respectively. Compared with pure MoB_2, which has a RRR of 2.74, these values point to increased scattering caused by alloying with Ta [8].

The $(Zr_{0.04}Mo_{0.96})_yB_2$ and $(Hf_{0.04}Mo_{0.96})_yB_2$ samples yielded notably higher T_c's than the Ta-substituted series with T_c^{onset}'s ranging from 6.31 to 8.60 K, with the latter belonging to $(Zr_{0.04}Mo_{0.96})_{0.85}B_2$ with a RRR of 1.04. These transition temperatures are comparable to the Zr-doped and Hf-doped results reported in Ref. [6]. The complete list of results for the RRR and T_c^{onset} is summarized in Table I.

C. Specific heat measurements

We characterize the low-temperature specific heat data using a Debye model given by

$$\frac{C}{T} = \gamma + \beta T^2, \tag{1}$$

TABLE I. Summary of experimental results for $([Ta/Zr/Hf/Nb]_yMo_{1-y})_xB_2$ in the $P6/mmm$ phase and for MoB_2 in the $R\bar{3}m$ phase. In arc-melted MoB_2, no superconductivity was observed down to 1.7 K, consistent with the literature [3]. The correct space groups for the ρ-bar and water-cooled splat-quenched MoB_2 samples are likely to be $R\bar{3}m$ but remain unknown. The DOS is stated per eV per formula unit. Abbreviations: a.m., arc-melted; ρ-bar, created using the ρ-bar cooling technique; w.c.s.q., water-cooled splat-quenched.

Material	Synthesis	T_c^{onset} (K)	T_c^{mid} (K)	$\frac{\Delta C}{\gamma T_c^{mid}}$	RRR	Measured a (Å)	Measured c (Å)	γ (mJ mol^{-1} K^2)	β (mJ mol^{-1} K^{-4})	Θ_D (K)	λ	$N^*(0)$ (states eV^{-1} f.u.$^{-1}$)	$N(0)$ (states eV^{-1} f.u.$^{-1}$)
$Ta_{0.1}Mo_{0.9}B_2$	a.m.	2.40	1.28	0.53	1.29	3.051	3.341	2.50	0.010	850	0.437	1.06	0.74
$Ta_{0.25}Mo_{0.75}B_2$	a.m.	2.48	1.42	0.64	1.13	3.081	3.308	2.47	0.052	480	0.485	1.05	0.71
$Ta_{0.4}Mo_{0.6}B_2$	a.m.	3.17	1.93	1.06	1.09	3.068	3.247	2.67	0.046	500	0.504	1.13	0.75
$Ta_{0.5}Mo_{0.5}B_2$	a.m.	2.46	1.70	0.99	1.09	3.068	3.249	2.65	0.111	370	0.509	1.12	0.74
$Zr_{0.04}Mo_{0.96}B_2$	a.m.	7.47	4.72	1.01	1.12	3.052	3.349	3.53	0.013	760	0.555	1.50	0.96
$(Zr_{0.04}Mo_{0.96})_{0.85}B_2$	a.m.	8.60	7.65	1.32	1.04	3.064	3.371	3.50	0.015	710	0.585	1.48	0.94
$(Zr_{0.04}Mo_{0.96})_{0.85}B_2$	ρ-bar	9.60	7.09	1.09	1.07			3.12	0.017	690	0.607	1.32	0.82
$(Zr_{0.04}Mo_{0.96})_{0.85}B_2$	w.c.s.q.	10.14			1.08								
$Hf_{0.04}Mo_{0.96}B_2$	a.m.	6.31	4.07	0.97	1.15	3.052	3.344	3.35	0.006	970	0.507	1.42	0.94
$(Hf_{0.04}Mo_{0.96})_{0.85}B_2$	a.m.	8.45	7.27	1.25	1.07	3.045	3.345	3.40	0.017	690	0.587	1.44	0.91
MoB_2 ($R\bar{3}m$)	a.m.	<1.7	<1.7		2.74								
MoB_2	ρ-bar	4.45	4.08	0.76	1.23			5.11	0.135	350	0.592	2.17	1.36
MoB_2	w.c.s.q.	4.55			1.28								
$MoB_{2.5}$	a.m.	3.06			1.38								
$MoB_{2.5}$	ρ-bar	5.82	2.88	0.76	1.10			3.36	0.130	810	0.517	1.43	0.94
$Nb_{0.25}Mo_{0.75}B_2$	a.m.	8.05	6.84	1.00	1.07	3.055[8]	3.264[8]	3.79	0.014	740	0.569	1.61	1.02
$Nb_{0.25}Mo_{0.75}B_2$	ρ-bar	10.67	8.44	0.89	1.10			3.94	0.016	710	0.620	1.67	1.03
$Nb_{0.25}Mo_{0.75}B_2$	w.c.s.q.	10.45			1.07								

where γ and β represent the linear (electronic) and cubic (phonon-related) specific heat coefficients, respectively. The fitting coefficients were obtained using an entropy-matching approach, ensuring the integral of C/T versus T from zero to T_c^{onset} in the superconducting state corresponds precisely to its integral in the normal state. From our estimated β value, we calculated the Debye temperature $\Theta_D = (12\pi^4 NR/5\beta)^{1/3}$, where N denotes the number of atoms per formula unit and R is the universal gas constant. We determined the linear specific heat coefficient $\gamma = \lim_{T\to 0} C_{normal}/T$, which is proportional to the renormalized electronic density of states (DOS) at the Fermi energy, denoted as $N^*(0)$.

Applying Landau Fermi-liquid theory [13], we approximated the experimental (renormalized) linear specific heat coefficient as $\gamma = \gamma^{(0)}(1+\lambda_m)$, where $\gamma^{(0)}$ is the noninteracting case's linear coefficient and λ_m captures the electron mass enhancement factor near the Fermi level [14]. In principle, λ_m includes effects from more than just electron-phonon interactions, but in our work, we assume the other effects are small. Hence, we take $\lambda_m \approx \lambda$ to estimate the renormalized and bare DOS $N(0)$, where λ is the electron-phonon coupling constant defined later. Using this approximation, the relationship between the renormalized and bare electronic DOS γ and λ is given as

$$\gamma = \frac{\pi^2 k_B^2}{3} N^*(0) = \frac{\pi^2 k_B^2}{3} N(0)(1+\lambda). \tag{2}$$

We report these values in the last column of Table I.

We gauged the bulk superconductivity by the ratio $\Delta C/(\gamma T_c^{mid})$, which equals a value of 1.43 in BCS superconductivity and, e.g., 1.65 in the unconventional, iron-based superconductor FeSe with $T_c = 8.1$ K [15]. Here, T_c^{mid} is obtained from the peak of the entropy-matched Debye fit on the specific heat data (see Table I). Assuming that $\Delta C/(\gamma T_c^{mid}) \approx$ 1.5 indicates 100% bulk superconductivity, the Ta-doped series shows 35% to 71% bulk superconductivity, similar to Nb-doped MoB_2 [8]. In contrast, the $(Zr_{0.04}Mo_{0.96})_yB_2$ and $(Hf_{0.04}Mo_{0.96})_yB_2$ compositions exhibit 67% to 88% and 65% to 83% bulk superconductivity, respectively. We list the ratios and values for γ, β, and Θ_D for each composition in Table I.

D. Estimate of the electron-phonon coupling

Equipped with T_c from the resistivity results and the Debye temperature from the specific heat fits, we estimate the electron-phonon coupling constant λ using the inverted McMillan formula [16]

$$\lambda = \frac{1.04 + \mu^* \ln[\Theta_D/(1.45T_c)]}{(1-0.62\mu^*)\ln[\Theta_D/(1.45T_c)] - 1.04}, \tag{3}$$

where μ^* is the Coulomb pseudopotential parameter. For better comparison, we follow Yang *et al.* [7] and Quan *et al.* [17] and take $\mu^* = 0.13$. For our samples involving Ta-, Zr-, Hf, and Nb-substituted MoB_2, we report the estimates for λ in Table I. The value of $\mu^* = 0.13$ sits in the middle of the range 0.1 to 0.15, a standard reference range for diborides [17]. Using the limits of this range, the estimates for λ will decrease by roughly 0.06 for $\mu^* = 0.1$ and increase by 0.04 for $\mu^* = 0.15$ compared with our choice of $\mu^* = 0.13$.

Regardless of the specific choice of μ^*, the procedure above indicates that, on the whole, nearly all the compounds studied in this work have λ between 0.4 and 0.65, consistent with similar estimates on many TM diborides [7,18,19]. This range of values is considered to be relatively weak by electron-phonon (e-ph) coupling standards.

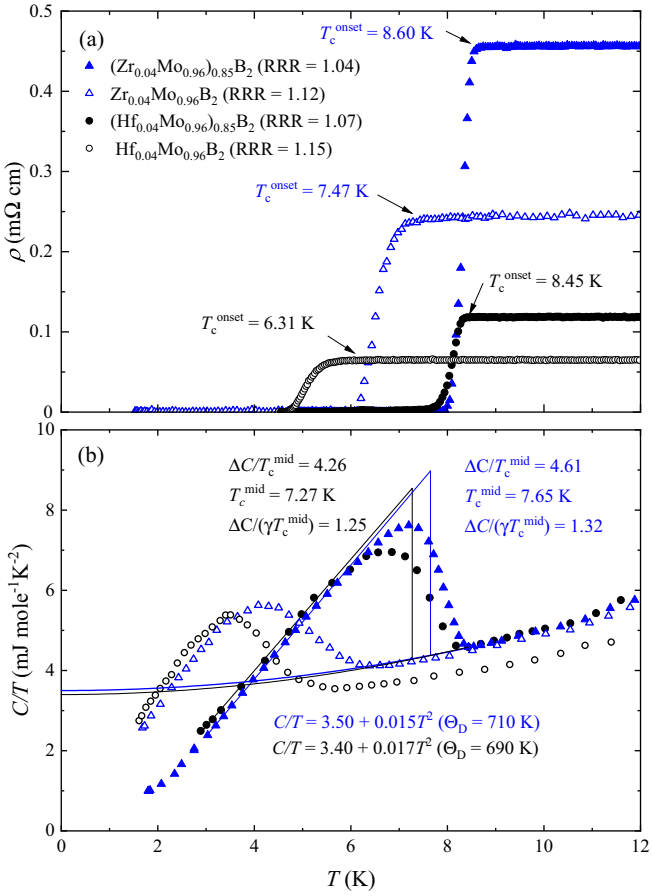

FIG. 4. Experimental results for the $(Zr_{0.04}Mo_{0.96})_yB_2$ and $(Hf_{0.04}Mo_{0.96})_yB_2$ systems for $y = 0.85$ and 1.00. (a) shows the resistivity measurements (in mΩ cm), and (b) shows the specific heat per unit temperature (in mJ mol^{-1} K^{-2}) for each composition. In (b), black and blue lines represent the Debye model fit obtained for the $y = 0.85$ samples.

E. Comparison with other alloyed MoB_2 compounds

Incorporating our recent measurements on the Ta-, Zr-, and Hf-substituted compounds with our earlier results on the $Nb_xMo_{1-x}B_2$ system and the findings from Refs. [6,7] regarding Zr- and Sc-doped MoB_2 alloys, we compiled a comprehensive summary of compositionally similar results to date. Utilizing the nominal composition and specific heat measurements, we sought potential correlations between the superconducting transition temperature T_c and the key properties of each system. These include the non-Mo TM-element doping x, linear specific heat contribution γ, Debye temperature Θ_D, and the e-ph coupling strength λ, as illustrated in Fig. 5.

Scrutiny of Fig. 5 reveals a weak correlation between T_c and the evaluated parameters, except for a modest association with λ. However, this modest correlation may arise from our empirical approach to estimating λ using Eq. (3) instead of a full *ab initio* evaluation. In our prior study on $Nb_xMo_{1-x}B_2$, *ab initio* estimates of T_c via density functional theory and the Allen-Dynes formula [20] consistently exceeded experimental results by a factor of 2 or more [9]. We proposed potential sources of this discrepancy, such as sample inhomogeneity, perhaps best exemplified by the formation of vacancies and stacking faults in transition metal diborides [6]. Regardless of the underlying cause, our data strongly suggest that these compounds exhibit weak coupling superconductivity under ambient pressure conditions.

Noticeably absent from Fig. 5 are nonstoichiometric results in which the ratio of boron to the TM atoms is greater than 2:1. We include a separate comparison of T_c's among these materials in Table II. There, we also include similar compositions from a few sources in the literature.

IV. ANALYSIS OF RAPIDLY COOLED SAMPLES

The early work by Cooper *et al.* [3] used splat quenching to make MoB_2, as typical arc melting seemed to produce a slightly B-deficient sample. However, their quenched MoB_2 sample did not exhibit superconductivity down to the lowest

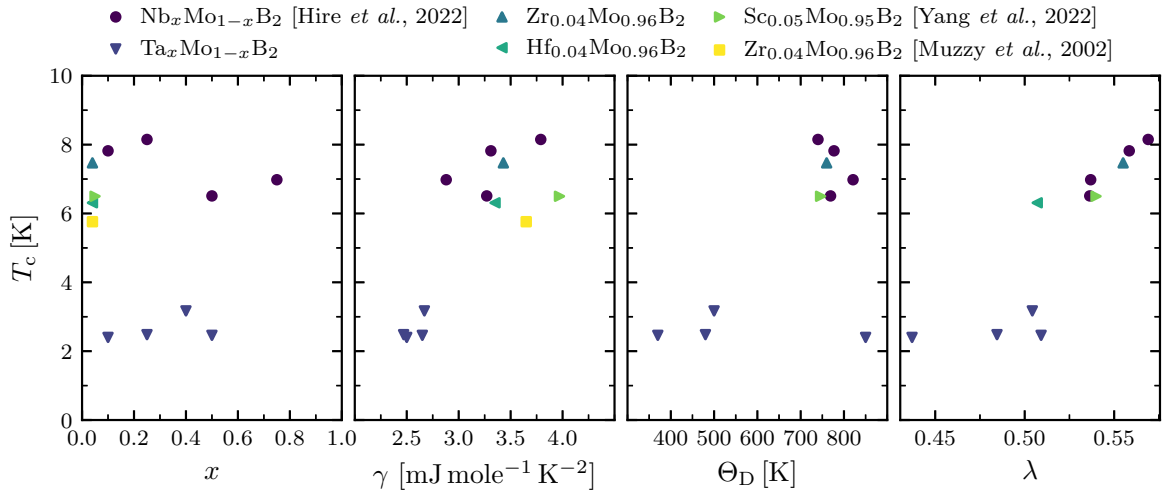

FIG. 5. Correlations of T_c with various quantities for various TM-substituted MoB_2 samples. Literature values are included from Refs. [8] (Nb), [6] (Zr), and [7] (Sc). In Ref. [7], the authors report $T_c^{mid} = 4.62$ K instead of T_c^{onset}. To be consistent, we plot an estimate of $T_c^{onset} \approx 6.5$ K from their resistivity data.

TABLE II. Survey of excess boron compositions of the form $(M_yMo_{1-y})_xB_2$, where $x = 0.8$ to 0.85 and $y \approx 0.4$–0.5, except for one entry with $M =$ Nb at 95% from Ref. [6]. Abbreviations: a.m., arc-melted; ρ-bar, created using the ρ-bar cooling technique; w.c.s.q., water-cooled splat-quenched.

Material	Synthesis	T_c^{onset} (K)	T_c^{mid} (K)	Ref.
$(Zr_{0.04}Mo_{0.96})_{0.85}B_2$	a.m.	8.60	7.65	This work
$(Zr_{0.04}Mo_{0.96})_{0.85}B_2$	ρ-bar	9.60	7.09	This work
$(Zr_{0.04}Mo_{0.96})_{0.85}B_2$	w.c.s.q.	10.14		This work
$(Zr_{0.04}Mo_{0.96})_{0.85}B_2$	a.m.	8.137		[6]
$(Hf_{0.04}Mo_{0.96})_{0.85}B_2$	a.m.	8.45	7.27	This work
$(Hf_{0.04}Mo_{0.96})_{0.80}B_2$	a.m.	~8.0		[6]
$(Ta_{0.04}Mo_{0.96})_{0.80}B_2$	a.m.	<4.0		[6]
$(W_{0.04}Mo_{0.96})_{0.80}B_2$	a.m.	<4.0		[6]
$(Nb_{0.95}Mo_{0.05})_{0.80}B_2$	a.m.	~3.5		[6]
$(Ti_{0.04}Mo_{0.96})_{0.80}B_2$	a.m.	5.0		[6]
$(Ti_{0.04}Mo_{0.96})_{0.80}B_2$	a.m.	7.4	7.0[a]	[21]
$(Sc_{0.05}Mo_{0.95})_{0.83}B_2$	a.m.	6.01		[7]

[a]Midpoint obtained from resistivity drop and not specific heat peak.

temperature measured, 1.8 K. Only for a splat-quenched sample of $MoB_{2.5}$ did they observe a transition ($T_c = 8.1$ K). We have reexamined the potential of rapid cooling during synthesis to generate favorable conditions for superconductivity in MoB_2 at *ambient* pressure. Surprisingly, both rapidly cooled MoB_2 samples exhibited superconductivity. As measured from the initial drop in the resistivity, the ρ-bar and water-cooled splat-quenched samples had T_c's of 4.45 and 4.55 K, respectively [see Fig. 6(a)]. Additional high-temperature resistivity data for the arc-melted and ρ-bar samples are featured in Fig. S5 in the Supplemental Material.

We measured the specific heat of the ρ-bar sample, and the result is plotted in Fig. 6(b). The specific heat jump is broad, and the Debye entropy-matching procedure yields $\gamma = 5.11$ mJ mol^{-1} K^{-2} and $\Theta_D = 350$ K. With $\Delta C/(\gamma T_c^{mid}) = 0.76$, we can assume that around 50% of the sample is superconducting. This may be the first observation of superconductivity in stoichiometric ambient pressure MoB_2 if excess boron can be ruled out. To better distinguish our MoB_2 from an excess boron phase, we also synthesized arc-melted and ρ-bar samples of $MoB_{2.5}$.

Figure 7 shows the XRD results for MoB_2 and $MoB_{2.5}$. The top and bottom XRD patterns are the theoretical results for MoB_2 in $P6/mmm$ ("α phase") and $R\bar{3}m$ ("β phase"), respectively. The arc-melted MoB_2 sample is better aligned with the $R\bar{3}m$ [166] structure, as expected [5,17]. The XRD results for the ρ-bar MoB_2 sample are far less conclusive. Unfortunately, the ill-defined peaks of the ρ-bar XRD pattern make it difficult to assign a structural phase. A few discernible peaks align somewhat with the $R\bar{3}m$ phase, but the lowest-angle peak better matches that of the $P6/mmm$ phase. This may indicate a mixture of $R\bar{3}m$ and $P6/mmm$-like defects analogous to the pressure-induced stacking faults in WB_2 [22]. The lack of a clear match in the XRD results implies that the precise stoichiometry is uncertain. Our nominal composition is based solely on the ratios of the constituents used in the arc-melting process. In comparison, the XRD results for $MoB_{2.5}$ have

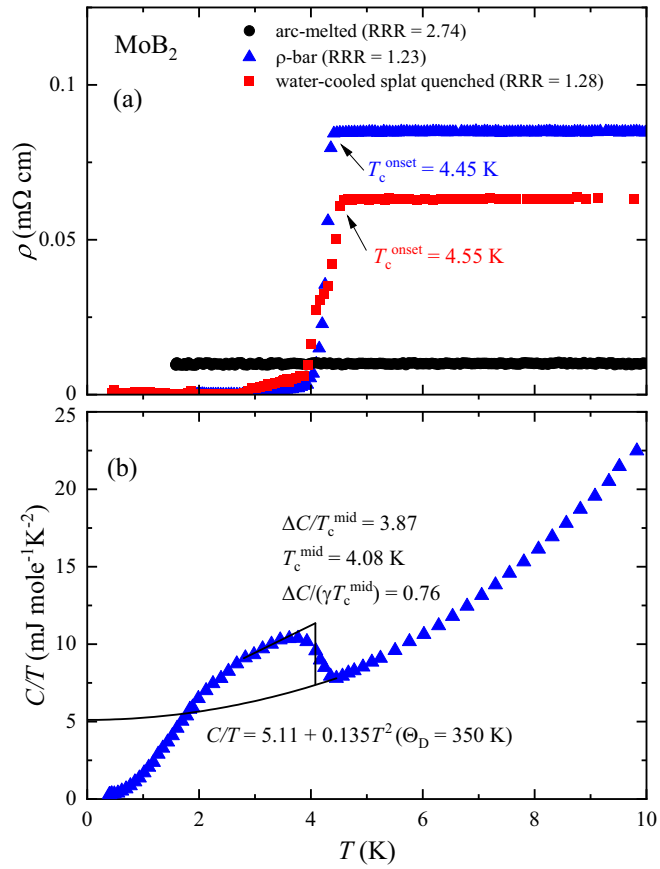

FIG. 6. Experimental results for MoB_2 showing (a) the resistivity ρ (in mΩ cm) for the arc-melted, ρ-bar, and water-cooled splat-quenched samples, as well as (b) the specific heat per unit temperature C/T (in mJ mol^{-1} K^{-2}) for only the ρ-bar sample.

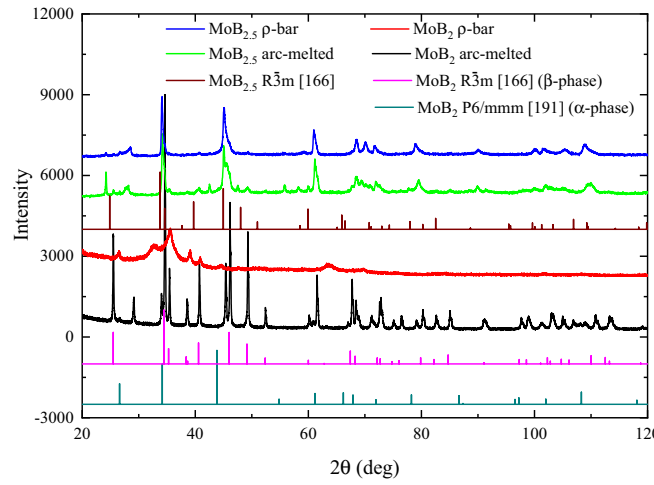

FIG. 7. X-ray diffraction measurements for MoB_2 and $MoB_{2.5}$ prepared by arc melting and the ρ-bar (rapid cooling) synthesis procedure. The bottom two diffraction patterns are the theoretical XRD results for MoB_2 in the $P6/mmm$ [191] and $R\bar{3}m$ [166] phases, respectively. The theoretical XRD results for $MoB_{2.5}$ in the $R\bar{3}m$ [166] phase are also included as the third entry from the top (reddish-brown lines).

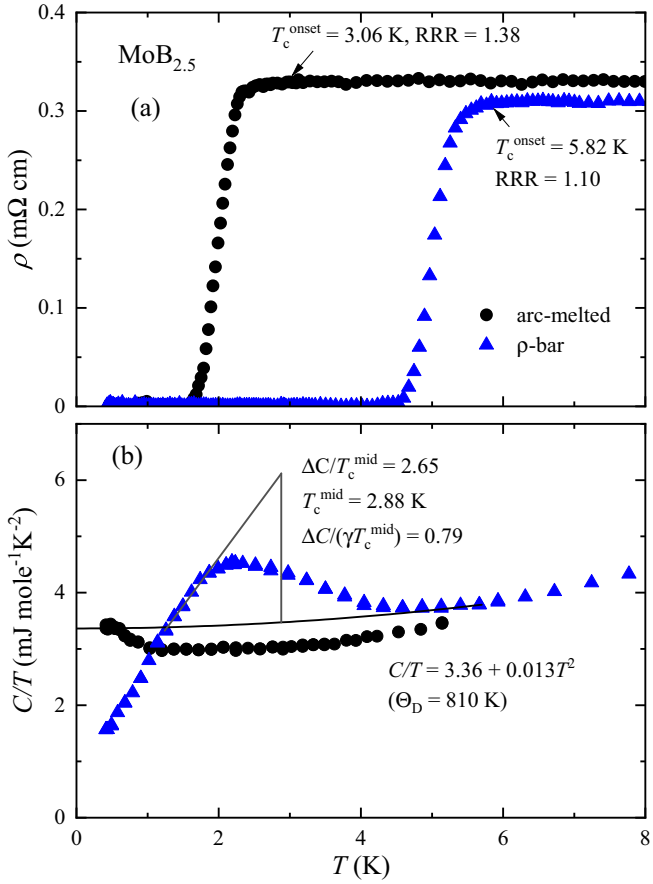

FIG. 8. Experimental results for $MoB_{2.5}$ showing (a) the resistivity ρ (in mΩ cm) and (b) the specific heat per unit temperature C/T (in mJ mole^{-1} K^{-2}) for the arc-melted and ρ-bar samples.

well-defined peaks and reveal that the arc-melted and ρ-bar samples are in the $P6/mmm$ [191] phase. These results are quite distinct from those of ρ-bar MoB_2, helping to rule out excess boron in the latter.

Nevertheless, using Eq. (3), we estimated the electron-phonon coupling constant in our ρ-bar sample MoB_2 to be $\lambda \approx 0.59$. This empirical value should be interpreted cautiously, especially when compared to recent *ab initio* calculations for the α phase under 90 GPa pressure, which suggest a λ range of approximately 1.6 to 1.71 [5,17,23]. These sources do not report a value for λ in the lower-pressure β phase. However, Ref. [5] reported a theoretical T_c of 5 K, implying λ is likely much smaller than that of the α phase under pressure. They ascribed the low T_c to a reduced electronic DOS at the Fermi level. The high-pressure phase is predicted to feature a larger electronic DOS near the Fermi level, thanks mostly to the presence of Van Hove singularities attributed to Mo d_{z^2} bands [23]. However, the high-pressure phase is also predicted to have a boosted contribution from boron p bands, which may have an outsized effect on increasing T_c [17]. Using the experimental results for the ρ-bar MoB_2, we estimate the renormalized (bare) DOS near the Fermi level to be $N^*(0) \approx 2.17$ states eV^{-1} f.u.$^{-1}$ [$N(0) \approx 1.36$ states eV^{-1} f.u.$^{-1}$].

In Fig. 8(a), we show our results for the resistivity of each $MoB_{2.5}$ sample. These arc-melted and ρ-bar samples have a broader transition than the ρ-bar MoB_2 with $T_c^{onset} = 3.06$ and 5.82 K, respectively. Moreover, the $MoB_{2.5}$ samples have higher resistivity above T_c^{onset} and lower RRR values, suggesting they contain more defects. Without further analysis, it is difficult to characterize the nature of these defects, although the possible phases and role and whereabouts of the excess boron have been argued in previous studies [10,24].

The specific heat measurements of the arc-melted and ρ-bar $MoB_{2.5}$ samples are shown in Fig. 8(b). The specific heat peak of the arc-melted samples (black circles) was not fully resolvable down to 0.41 K, and the addenda contribution approaches 50% at the highest temperature of 5.2 K. The ρ-bar samples (blue triangles) show a fairly broad peak, and the entropy-matching procedure places T_c^{mid} at 2.88 K, considerably lower than the main drop in resistivity. The Debye coefficients are $\gamma = 3.36$ mJ mol^{-1} K^{-2} and $\beta = 0.013$ mJ mol^{-1} K^{-4}, the latter leading to a Debye temperature of $\Theta_D = 810$ K. These results lead to a slightly weaker $\lambda \sim 0.52$ and DOS at the Fermi level compared with the MoB_2 ρ-bar samples (see Table I).

Turning our focus to the $(Zr_{0.04}Mo_{0.96})_{0.85}B_2$ composition, which exhibited the highest transition temperature (T_c = 8.60 K) of the arc-melted samples, we undertook further synthesis using the ρ-bar and water-cooled splat-quenching methods. Our XRD measurements (see Supplemental Material, Fig. S2) indicate these samples have the $P6/mmm$ [191] space group structure. The resistivity and specific heat results are shown in Fig. 9. The water-cooled splat-quenched sample yielded a slightly higher T_c^{onset} of 10.14 K compared with the ρ-bar sample $T_c^{onset} = 9.60$ K [Fig. 9(a)]. However, both have broader resistivity drops compared with the arc-melted sample. This trend is further exemplified by comparing the specific heat jumps of the arc-melted and ρ-bar samples in Fig. 9(b). The arc-melted sample displays more bulk superconductivity, with $\Delta C/(\gamma T_c^{mid}) \sim 1.32$, compared with 1.09 in the ρ-bar system. We determine $\Theta_D = 710$ and 690 K for the arc-melted and ρ-bar samples from the Debye fitting procedure. Our estimate for the e-ph coupling is $\lambda \approx 0.61$, the largest estimate obtained thus far, although it is relatively weak.

We synthesized ρ-bar and water-cooled splat-quenched samples of $Nb_{0.25}Mo_{0.75}B_2$. Our XRD results (see Supplemental Material, Fig. S3) confirm they have $P6/mmm$ [191] space group symmetry. The resistivity measurements are plotted in Fig. 10(a). These curves reveal a considerable spread among the samples. The transition for the arc-melted sample starts at $T_c^{onset} = 8.05$ K, followed by the water-cooled splat-quenched sample with $T_c^{onset} = 10.45$ K and topped by the ρ-bar sample with $T_c = 10.67$. These samples exhibit similar RRR values, ranging from 1.07 to 1.10. Compared to the arc-melted sample, the ρ-bar and water-cooled splat-quenched samples show broader transitions. This observation is most evident when comparing their specific heat measurements, as shown in Fig. 10(b). The ρ-bar sample exhibits a lower $\Delta C/(\gamma T_c^{mid})$ ratio of 0.89, as opposed to 1.00 for the arc-melted sample. The linear specific heat coefficients were $\gamma = 3.79$ and 3.94 mJ mol^{-1} K^{-2} for the arc-melted and ρ-bar samples, respectively. Additionally, the Debye temperatures

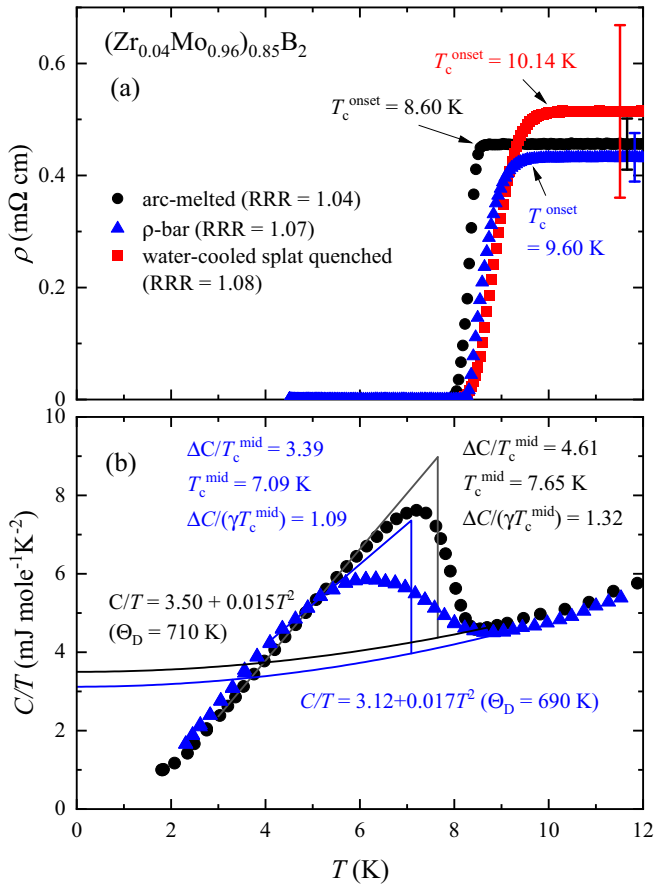

FIG. 9. Experimental results for $(Zr_{0.04}Mo_{0.96})_{0.85}B_2$ showing (a) the resistivity ρ (in mΩ cm) for the arc-melted, ρ-bar, and water-cooled splat-quenched samples, as well as (b) the specific heat per unit temperature C/T (in mJ mol^{-1} K^{-2}) for the arc-melted and ρ-bar samples.

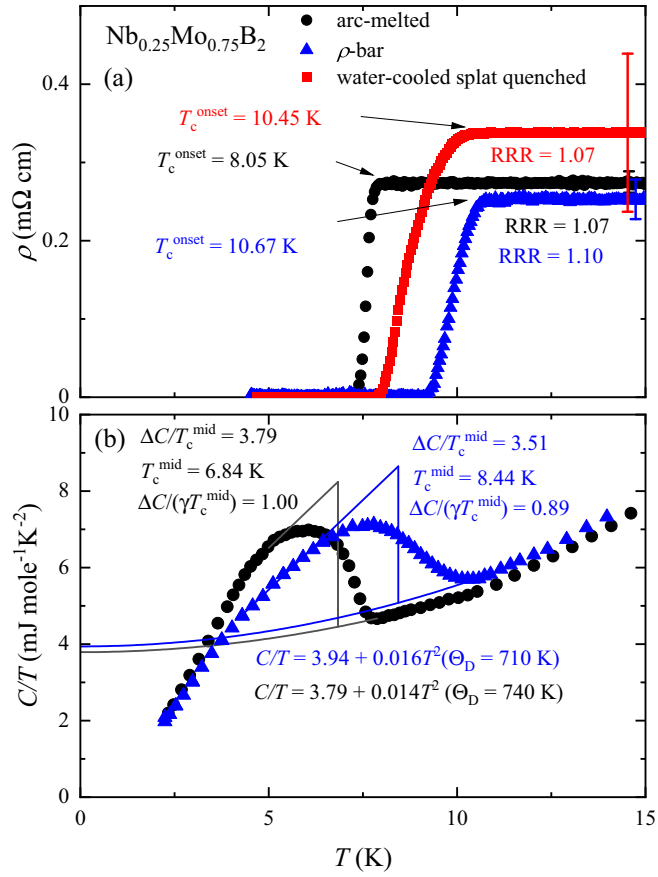

FIG. 10. Experimental results for $Nb_{0.25}Mo_{0.75}B_2$ showing (a) the resistivity ρ (in mΩ cm) for the arc-melted, ρ-bar, and water-cooled splat-quenched samples, as well as (b) the specific heat per unit temperature C/T (in mJ mol^{-1} K^{-2}) for the arc-melted and ρ-bar samples.

Θ_D were found to be 740 and 710 K for the arc-melted and ρ-bar samples, respectively.

V. DISCUSSION

Our experiments reveal that rapid cooling synthesis methods, such as the ρ-bar and water-cooled splat-quenched techniques, yield higher transition temperatures T_c than arc-melted samples. This effect becomes especially pronounced in the case of MoB_2, which is not considered [3] superconducting at ambient pressure. Here, rapid cooling induces a significant superconducting transition at approximately 4.5 K. Curiously, this matches quite well the theoretical prediction of 5 K for the β-phase MoB_2 at ambient pressure [5]. For alloys like $(Zr_{0.04}Mo_{0.96})_{0.85}B_2$ and $Nb_{0.25}Mo_{0.75}B_2$, the increase in T_c is less dramatic. However, these samples show some evidence of inhomogeneities, resulting in lower $\Delta C/(\gamma T_c^{mid})$ ratios.

A limitation of our study is the lack of detailed information about the precise structure and composition of the ρ-bar and splat-quenched MoB_2 samples. Understanding the exact B:Mo ratio would provide crucial context for the significance of our findings. Consistent with the literature [3], we found that $MoB_{2.5}$ is superconducting and is experimentally quite distinct from MoB_2. The arc-melted and ρ-bar $MoB_{2.5}$ samples predominantly show the $P6/mmm$ phase and exhibit broader superconducting transitions. Our results potentially offer evidence of ambient pressure superconductivity in MoB_2. A careful study of the superconductivity under pressure would be a logical next step. There, we could determine whether our MoB_2 samples follow a dT_c/dP trend analogous to that discovered by Pei *et al.* [5] or something else entirely. Whether or not TM-substituted MoB_2 or other TM diborides can achieve similar high-T_c values under lower applied pressure than MoB_2 remains to be seen.

While our study primarily investigates the superconducting properties of MoB_2 and its various alloys, it is important to recognize the broader context. Borides and diborides have long been known to have exemplary high-temperature properties such as high hardness, robust oxidation resistance, and high melting points [25–34]. Recently, they started attracting interest for their low-temperature topological features. A notable example is the emergence of Dirac cones in the electronic structure of monolayer diborides, as highlighted in studies on TiB_2 [35], FeB_2 [36], and ZrB_2 [37]. Adding to this are recently discovered topological features in the phonon spectrum of α-MoB_2, revealing parity-time symmetry-protected helical nodal lines [38]. Such topological

states give rise to phononic boundary modes on the surface unaffected by local disorder. However, exploring the potential relevance of this topology of electronic and bosonic states in alloyed TM diborides, like the ones featured in this work, is still a nascent topic.

VI. CONCLUSIONS

In this work, we report our experimental results for several TM-substituted MoB_2 superconductors. Motivated by the recent finding of pressure-induced superconductivity up to 32 K in MoB_2, we investigated the potential for chemical substitution and rapid cooling to generate metastable superconductivity at ambient pressure. As others showed in previous works, alloying MoB_2 with other TMs—especially those with fewer d electrons than Mo—can help to stabilize the AlB_2 $P6/mmm$ space group structure at ambient pressure. Substitutions of 10% to 50% Ta and 4% Hf yield superconducting alloys with T_c's near 2.4–3.2 and 6.3 K, respectively. We also examined Zr-substituted MoB_2 at 4%, finding $T_c \sim$ 7.5 K, similar to older results by Muzzy *et al.* [6]. Collectively, the role of TM substitution into MoB_2, particularly for elements with fewer d electrons, is to introduce stability by suppressing the antibonding character of dominant Mo-Mo bonds at the Fermi level [6,24,39]. One consequence of rapid quenching may be to enhance the electron-phonon coupling λ, but this increase may occur for different reasons in each material. Rapid cooling appears to lower the Debye temperature in each sample; however, the linear specific heat coefficient trends oppositely in the Nb-doped and excess boron Zr-doped samples.

The nature and concentration of defects in these samples are almost certainly affected by the speed of the rapid cooling synthesis. Vacancies [18,28,40] and stacking faults [6,22] are likely responsible for variations in T_c in similar TM diborides. How these defects form under different cooling rates and their role in metastable superconductivity remains an open question.

As expected from the literature, our arc-melted MoB_2 was not superconducting down to 1.7 K. However, two rapidly cooled samples exhibited superconductivity at ambient pressure with $T_c^{\text{onset}} \sim 4.5$ K. Although we could not estimate the precise composition and structure from XRD measurements, we showed they are distinct from a known excess boron composition $MoB_{2.5}$. Investigations into the precise composition and properties of rapidly cooled MoB_2 under high pressure are the subject of future work. Additional figures for this work are provided in the Supplemental Materials [41].

ACKNOWLEDGMENTS

Work at the University of Florida was performed under the auspices of the U.S. National Science Foundation, Division of Materials Research, under Contract No. NSF-DMR-2118718. A.C.H. and R.G.H. acknowledge support from the Center for Bright Beams, U.S. National Science Foundation (Award No. PHY-1549132.).

[1] J. Nagamatsu, N. Nakagawa, T. Muranaka, Y. Zenitani, and J. Akimitsu, Superconductivity at 39 K in magnesium diboride, Nature (London) **410**, 63 (2001).

[2] Y. S. Tyan, L. E. Toth, and Y. A. Chang, Low temperature specific heat study of the electron transfer theory in refractory metal borides, J. Phys. Chem. Solids **30**, 785 (1969).

[3] A. S. Cooper, E. Corenzwit, L. D. Longinotti, B. T. Matthias, and W. H. Zachariasen, Superconductivity: The transition temperature peak below four electrons per atom, Proc. Natl. Acad. Sci. USA **67**, 313 (1970).

[4] L. Leyarovska and E. Leyarovski, A search for superconductivity below 1 k in transition metal borides, J. Less-Common Met. **67**, 249 (1979).

[5] C. Pei, J. Zhang, Q. Wang, Y. Zhao, L. Gao, C. Gong, S. Tian, R. Luo, M. Li, W. Yang, Z.-Y. Lu, H. Lei, K. Liu, and Y. Qi, Pressure-induced superconductivity at 32 K in MoB_2, Natl. Sci. Rev. **10**, nwad034 (2023).

[6] L. E. Muzzy, M. Avdeev, G. Lawes, M. K. Haas, H. W. Zandbergen, A. P. Ramirez, J. D. Jorgensen, and R. J. Cava, Structure and superconductivity in Zr-stabilized, nonstoichiometric molybdenum diboride, Phys. C (Amsterdam, Neth.) **382**, 153 (2002).

[7] W. Yang, G. Xiao, Q. Zhu, Y. Cui, S. Song, G.-H. Cao, and Z. Ren, Stabilization and superconductivity of AlB_2-type nonstoichiometric molybdenum diboride by Sc doping, Ceram. Int. **48**, 19971 (2022).

[8] A. C. Hire, S. Sinha, J. Lim, J. S. Kim, P. M. Dee, L. Fanfarillo, J. J. Hamlin, R. G. Hennig, P. J. Hirschfeld, and G. R. Stewart, High critical field superconductivity at ambient pressure in MoB_2 stabilized in the P6/mmm structure via Nb substitution, Phys. Rev. B **106**, 174515 (2022).

[9] J. Lim, S. Sinha, A. C. Hire, J. S. Kim, P. M. Dee, R. S. Kumar, D. Popov, R. J. Hemley, R. G. Hennig, P. J. Hirschfeld, G. R. Stewart, and J. J. Hamlin, Niobium substitution suppresses the superconducting critical temperature of pressurized MoB_2, Phys. Rev. B **108**, 094501 (2023).

[10] J. K. Burdett, E. Canadell, and G. J. Miller, Electronic structure of transition-metal borides with the AlB_2 structure, J. Am. Chem. Soc. **108**, 6561 (1986).

[11] G. R. Stewart, Measurement of low-temperature specific heat, Rev. Sci. Instrum. **54**, 1 (1983).

[12] A. Jain, S. P. Ong, G. Hautier, W. Chen, W. D. Richards, S. Dacek, S. Cholia, D. Gunter, D. Skinner, G. Ceder, and K. A. Persson, Commentary: The Materials Project: A materials genome approach to accelerating materials innovation, APL Mater. **1**, 011002 (2013).

[13] P. Coleman, *Introduction to Many-Body Physics* (Cambridge University Press, Cambridge, 2015).

[14] Formally, $\lambda_m := -d\Sigma(\omega)/d\omega|_{\omega=0}$, where $\Sigma(\omega)$ is the electron self-energy averaged over the Fermi surface $\Sigma(\omega) := \langle \Sigma(\mathbf{k}, \omega) \rangle_{\mathbf{k}\in \text{FS}}$.

[15] J.-Y. Lin, Y. S. Hsieh, D. A. Chareev, A. N. Vasiliev, Y. Parsons, and H. D. Yang, Coexistence of isotropic and extended s-wave order parameters in FeSe as revealed by low-temperature specific heat, Phys. Rev. B **84**, 220507(R) (2011).

[16] W. L. McMillan, Transition temperature of strong-coupled superconductors, Phys. Rev. **167**, 331 (1968).

[17] Y. Quan, K.-W. Lee, and W. E. Pickett, MoB_2 under pressure: Superconducting Mo enhanced by boron, Phys. Rev. B **104**, 224504 (2021).

[18] I. R. Shein and A. L. Ivanovskii, Influence of lattice vacancies on the structural, electronic, and cohesive properties of niobium and molybdenum borides from first-principles calculations, Phys. Rev. B **73**, 144108 (2006).

[19] R. Heid, B. Renker, H. Schober, P. Adelmann, D. Ernst, and K.-P. Bohnen, Lattice dynamics and electron-phonon coupling in transition-metal diborides, Phys. Rev. B **67**, 180510(R) (2003).

[20] P. B. Allen and R. C. Dynes, Transition temperature of strong-coupled superconductors reanalyzed, Phys. Rev. B **12**, 905 (1975).

[21] W. Yang, G. Xiao, Q. Zhu, S. Song, G.-H. Cao, and Z. Ren, Effect of carbon doping on the structure and superconductivity in AlB_2-type $(Mo_{0.96}Ti_{0.04})_{0.8}B_2$, J. Am. Ceram. Soc. **106**, 4211 (2023).

[22] J. Lim, A. C. Hire, Y. Quan, J. S. Kim, S. R. Xie, S. Sinha, R. S. Kumar, D. Popov, C. Park, R. J. Hemley, Y. K. Vohra, J. J. Hamlin, R. G. Hennig, P. J. Hirschfeld, and G. R. Stewart, Creating superconductivity in WB_2 through pressure-induced metastable planar defects, Nat. Commun. **13**, 7901 (2022).

[23] X. Liu, X. Huang, P. Song, C. Wang, L. Zhang, P. Lv, L. Liu, W. Zhang, J.-H. Cho, and Y. Jia, Strong electron-phonon coupling superconductivity in compressed α-MoB_2 induced by double Van Hove singularities, Phys. Rev. B **106**, 064507 (2022).

[24] H. Klesnar, T. L. Aselage, B. Morosin, and G. H. Kwei, The diboride compounds of molybdenum: MoB_{2-x} and Mo_2B_{5-y}, J. Alloys Compd. **241**, 180 (1996).

[25] J. Castaing and P. Costa, *Boron and Refractory Borides*, edited by V. I. Matkovich (Springer, Berlin, 1977), pp. 390–412.

[26] E. Storms and B. Mueller, Phase relations and thermodynamic properties of transition metal borides. I. The molybdenum-boron system and elemental boron, J. Phys. Chem. **81**, 318 (1977).

[27] S. Okada, T. Atoda, I. Higashi, and Y. Takahashi, Preparation of single crystals of MoB_2 by the aluminium-flux technique and some of their properties, J. Mater. Sci. **22**, 2993 (1987).

[28] A. L. Ivanovskii, Mechanical and electronic properties of diborides of transition 3*d*–5*d* metals from first principles: Toward search of novel ultra-incompressible and superhard materials, Prog. Mater. Sci. **57**, 184 (2012).

[29] Q. Tao, X. Zhao, Y. Chen, J. Li, Q. Li, Y. Ma, J. Li, T. Cui, P. Zhu, and X. Wang, Enhanced Vickers hardness by quasi-3D boron network in MoB_2, RSC Adv. **3**, 18317 (2013).

[30] W. Hayami, A. Momozawa, and S. Otani, Effect of defects in the formation of AlB_2-type WB_2 and MoB_2, Inorg. Chem. **52**, 7573 (2013).

[31] X. Xu, K. Fu, M. Yu, Z. Lu, X. Zhang, G. Liu, and C. Tang, The thermodynamic, electronic and elastic properties of the early-transition-metal diborides with AlB_2-type structure: A density functional theory study, J. Alloys Compd. **607**, 198 (2014).

[32] L.-P. Ding, P. Shao, F.-H. Zhang, C. Lu, L. Ding, S. Y. Ning, and X. F. Huang, Crystal structures, stabilities, electronic properties, and hardness of MoB_2: First-principles calculations, Inorg. Chem. **55**, 7033 (2016).

[33] H. Tang, X. Gao, J. Zhang, B. Gao, W. Zhou, B. Yan, X. Li, Q. Zhang, S. Peng, D. Huang *et al.*, Boron-rich molybdenum boride with unusual short-range vacancy ordering, anisotropic hardness, and superconductivity, Chem. Mater. **32**, 459 (2020).

[34] M. Magnuson, L. Hultman, and H. Högberg, Review of transition-metal diboride thin films, Vacuum **196**, 110567 (2022).

[35] L. Z. Zhang, Z. F. Wang, S. X. Du, H.-J. Gao, and F. Liu, Prediction of a Dirac state in monolayer TiB_2, Phys. Rev. B **90**, 161402(R) (2014).

[36] H. Zhang, Y. Li, J. Hou, A. Du, and Z. Chen, Dirac state in the FeB_2 monolayer with graphene-like boron sheet, Nano Lett. **16**, 6124 (2016).

[37] A. Lopez-Bezanilla, Twelve inequivalent Dirac cones in two-dimensional ZrB_2, Phys. Rev. Mater. **2**, 011002(R) (2018).

[38] T. T. Zhang, H. Miao, Q. Wang, J. Q. Lin, Y. Cao, G. Fabbris, A. H. Said, X. Liu, H. C. Lei, Z. Fang, H. M. Weng, and M. P. M. Dean, Phononic helical nodal lines with $\mathcal{PT}$ protection in MoB_2, Phys. Rev. Lett. **123**, 245302 (2019).

[39] P. Vajeeston, P. Ravindran, C. Ravi, and R. Asokamani, Electronic structure, bonding, and ground-state properties of AlB_2-type transition-metal diborides, Phys. Rev. B **63**, 045115 (2001).

[40] H. Takeya, K. Togano, Y. S. Sung, T. Mochiku, and K. Hirata, Metastable superconductivity in niobium diborides, Phys. C (Amsterdam, Neth.) **408**, 144 (2004).

[41] See Supplemental Material at http://link.aps.org/supplemental/10.1103/PhysRevB.109.104520 for additional XRD measurements and high-temperature resistivity data.